

Subhra Datta
Sandip Ghosal
Neelesh A. Patankar

Department of Mechanical
 Engineering,
 Northwestern University, Evanston,
 USA

Received August 23, 2005
 Revised October 12, 2005
 Accepted October 17, 2005

Research Article

Electroosmotic flow in a rectangular channel with variable wall zeta-potential: Comparison of numerical simulation with asymptotic theory

Electroosmotic flow in a straight micro-channel of rectangular cross-section is computed numerically for several situations where the wall zeta-potential is not constant but has a specified spatial variation. The results of the computation are compared with an earlier published asymptotic theory based on the lubrication approximation: the assumption that any axial variations take place on a long length scale compared to a characteristic channel width. The computational results are found to be in excellent agreement with the theory even when the scale of axial variations is comparable to the channel width. In the opposite limit when the wavelength of fluctuations is much shorter than the channel width, the lubrication theory fails to describe the solution either qualitatively or quantitatively. In this short wave limit the solution is well described by Ajdari's theory for electroosmotic flow between infinite parallel plates (Ajdari, A., *Phys. Rev. E* 1996, 53, 4996–5005.) The infinitely thin electric double layer limit is assumed in the theory as well as in the simulation.

Keywords: Electroosmosis / Lubrication theory / Microfluidics / Zeta potential

DOI 10.1002/elps.200500618

1 Introduction

In the limit of infinitely thin Debye layers, the electroosmotic velocity inside a microfluidic channel of arbitrary shape is given by

$$u = \frac{\varepsilon\zeta}{4\pi\mu} \nabla\phi \quad (1)$$

provided no pressure difference is applied across it and there is no variation in the material properties of the channel or the fluid. Here ε is the dielectric constant of the fluid, ζ is the wall zeta-potential and μ is the fluid viscosity. ϕ is the potential due to the externally imposed voltage drop. This "similarity" of fluid velocity and electric field was first pointed out by Morrison in the context of electrophoresis of small uniformly charged particles [6]. The conclusion however is not true if the zeta-potential (or any of the other material constants) in Eq. (1) is spatially varying.

Spatially varying zeta-potentials are encountered in many applications. For example, when an electrophoretic channel is etched on a chip and bonded with a cover slip of a different material, the zeta-potential on one of the walls could differ from that on the other three. Axial gradients of the zeta-potential may be created when the channel adsorbs small amounts of the analyte [4]. In some recent applications, the possibility of deliberately imprinting variations of the zeta-potential to achieve certain functions (such as mixing) has been explored [9].

In the case of spatially varying zeta-potential exact analytical solutions of the fluid flow equations are not available except for certain special geometries. Analytical progress has been possible under one of two approximations (see the reviews [4, 9] and the included references):

- (i) the fluctuations of ζ are small compared to its characteristic value [5], and
- (ii) the characteristic scale of variation in the axial direction (L) over which the zeta-potential varies, is very much larger than the characteristic capillary width (w) – the lubrication approximation.

Correspondence: Subhra Datta, Department of Mechanical Engineering, Northwestern University, 2145 Sheridan Rd., Evanston, IL 60208, USA

E-mail: s-datta2@northwestern.edu

Fax: +1-847-491-3915

Abbreviation: EDL, electric double layer

The purpose of this paper is to test the accuracy of predictions based on the lubrication approximation by comparing predictions of the theory with numerical calculations on some representative flows in a channel of rectangular cross-section.

2 The test problem

Figure 1 shows the rectangular channel in cross-section. The width is $2b$ and height is $2c$. The x -axis; perpendicular to the plane of the paper and pointing inward, is along the longitudinal axis of the capillary. The length of the capillary is L . The zeta potentials on the walls AB, BC, CD and DA are $\zeta_{AB}(x)$, $\zeta_{BC}(x)$, $\zeta_{CD}(x)$ and $\zeta_{DA}(x)$, respectively; these parameters could vary with x but not with y or z . The flow velocity components in x , y and z directions are u , v and w , respectively. The following cases will be studied (here ζ_0 , ζ_1 , a , λ and $\Delta\zeta$ are given parameters):

Case A $\zeta_{AB} = \zeta_{CD} = \zeta_{DA} = \zeta_0$, $\zeta_{BC} = \zeta_1$

Case B $\zeta_{AB} = \zeta_{CD} = \zeta_{DA} = \zeta_0$, $\zeta_{BC} = \zeta_0 [1 - \exp(-ax)]$, $c/b = 1$

Case C $\zeta_{AB} = \zeta_{CD} = \zeta_{DA} = \zeta_0$, $\zeta_{BC} = \zeta_0 [1 - \exp(-ax)]$, $c/b = 1$

Case D $\zeta_{AB} = \zeta_{CD} = \zeta_{DA} = \zeta_0$, $\zeta_{BC} = \zeta_0 - \Delta\zeta \sin(2\pi x/\lambda)$, $c/b = 0.5$, $\lambda > 2b$

Case E $\zeta_{AB} = \zeta_{CD} = \zeta_{DA} = \zeta_0$, $\zeta_{BC} = \zeta_0 + \Delta\zeta \cos(2\pi x/\lambda)$, $c/b = 0.2$, $\lambda < 2b$

The configuration of Case A is motivated by the situation already mentioned in the introduction where an electrophoretic channel is made by bonding a cover slip on top of a channel etched on a substrate. Case B combines both features; the lack of equality of the zeta-potential on all four walls as well as axial variations of ζ on one of the walls. The exponential model for the axial variation could be representative of situations where there is a reduction in the zeta potential in the axial direction due to adsorp-

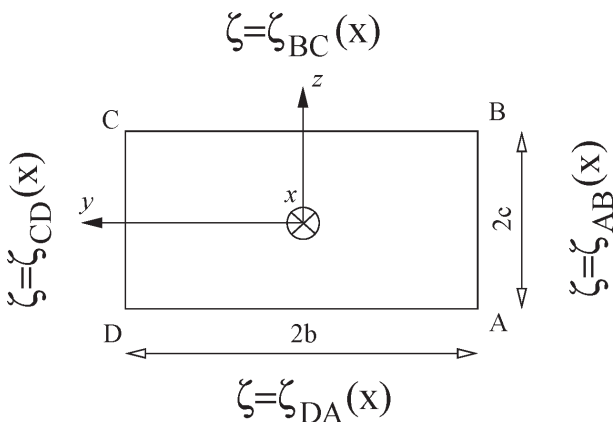


Figure 1. Geometry of the rectangular duct.

tion of contaminants from an analyte plug [3]. Case C is similar except that the effect of axial variations alone is studied. The sinusoidal fluctuation studied in Case D is useful because in the Stokes flow limit ($Re = 0$) the flow problem is linear. Thus, any problem involving axial variation in ζ could be reduced to a sequence of problems involving sinusoidal variations. Furthermore the sine profile gives a qualitative idea of how the flow properties might depend upon the amplitude and length scale of any fluctuation in ζ . Case E is similar to Case D except wavelengths much shorter than the channel width is considered where the lubrication approximation is expected to breakdown.

The flow is driven by a constant electric field E_0 , and the Helmholtz-Smoluchowski slip velocity for $\zeta = \zeta_0$:

$$u_0 = -\frac{\varepsilon\zeta_0 E_0}{4\pi\mu} \quad (2)$$

will be taken as a reference velocity. The width $2b$ will be taken as the reference length. Then the dimensionless parameters in this problem are: (a) the Reynolds number $Re = \rho u_0(2b)/\mu$ where ρ is the (constant) density of the fluid; (b) the aspect ratio, (c/b) ; (c) the dimensionless channel length, $L/(2b)$; (d) the parameter αL ; (e) the zeta potential ratio, ζ_1/ζ_0 ; (f) the dimensionless amplitude $\Delta\zeta/\zeta_0$ and (g) the ratio λ/L . Of these, two of the parameters will be held fixed: $Re = 1$ and $L/(2b) = 20$ (except for Case E which is discussed later). In microfluidic applications $Re \sim 1$, and further this scaling is implicit in the lubrication theory analysis we wish to check. For a $50 \mu\text{m}$ wide channel that is 2 cm long, $L/(2b) = 400$. Thus, a choice of 20 is much smaller than what would be considered typical. However we chose this lower value so as not to make the computational time unduly long. Further, if the lubrication theory works well here, its performance would only improve with a larger $L/2b$.

In Case E, the wavelength of the zeta potential distribution on the wall BC is a fraction of the channel width $2b$. The corresponding grid resolution requirements make the solution in a long channel ($L/(2b) \sim 20$) unduly expensive in terms of computational time. We therefore restrict ourselves to the case of Stokes flow ($Re = 0$), which has the advantage of not having a “development region” near the inlet section of the channel. Thus, we can consider a channel of short length, $L = 2b$, and apply the periodic boundary condition between the inlet and outlet. The actual physical channel may be constructed by joining a large number of these periodic units. An aspect ratio $c/b = 0.2$ was used.

The pressure difference between the inlet and outlet is assumed zero for all cases, of course in Case E the periodic boundary condition automatically ensures that it is

zero. One of the flow properties we are interested in is the electroosmotic mobility, μ_{eof} defined as $\bar{u} = \mu_{\text{eof}} E_0$ where \bar{u} is the volume flux per unit area (the average velocity). The mobility will always be quoted as a ratio $\mu_{\text{eof}}/\mu_{\text{eof}}^{\text{ref}}$ where $\mu_{\text{eof}}^{\text{ref}}$ is a “reference mobility” for a uniform channel with $\zeta = \zeta_0$. The dimensionless pressure gradient is defined as

$$\pi_* = -\frac{(2b)^2 d\bar{p}}{\mu u_0 dx} \quad (3)$$

Here, \bar{p} denotes the pressure averaged over the area of cross-section. All calculated results are presented in dimensionless form so that the actual physical values of parameters (such as the value of ζ_0) is never needed and never used in this paper.

3 Summary of analytical results

Lubrication theory (or the “Lubrication Limit”) is an asymptotic approach often employed in solving fluids problems where the fluid flows through a gap but the gap width is “slowly varying”; *i.e.* does not change much over distances of the order of the gap width itself. The name derives from one of the earliest applications of the theory to the flow of oil or other lubricant in the narrow gap between an axle and the shaft in which it rotates or between other moving parts in machinery [1]. The solution to the electroosmotic flow problem in a rectangular cross-section channel, when each wall is assigned a different x -dependent ζ potential has been worked out in the lubrication limit [2]. In our current notation, these results may be stated as follows:

$$u(x, y, z) = -\frac{u_p}{\mu} \frac{dp}{dx} + \frac{\varepsilon E_0 \psi}{4\pi\mu} \quad (4)$$

where u_p and ψ are known functions of position. For a rectangular cross-section

$$u_p(y, z) = \frac{1}{2}b^2 - \frac{1}{2}y^2 - 2b^2 \left(\frac{2}{\pi}\right)^3 \sum_{n=0}^{\infty} \frac{(-1)^n}{(2n+1)^3} \times \\ \times \frac{\cosh[(2n+1)(\pi z/2b)]}{\cosh[(2n+1)(\pi c/2b)]} \cos[(2n+1)(\pi y/2b)] \quad (5)$$

The potential ψ can be written as a superposition $\psi = \psi_{(AB)} + \psi_{(BC)} + \psi_{(CD)} + \psi_{(DA)}$ where $\psi_{(BC)}$ is the potential one would obtain if the side BC were held at a certain $\zeta = \zeta_{BC}$ and all of the other sides held at $\zeta = 0$. The other potentials $\psi_{(AB)}$, $\psi_{(CD)}$, $\psi_{(DA)}$ are defined similarly and can be obtained by symmetry from ψ_{BC} :

$$\psi_{(BC)}(y, z) = -\sum_{n=0}^{\infty} \frac{4\zeta_{BC}}{(2n+1)\pi} \frac{\sinh\left[\frac{(2n+1)\pi}{2b}(z+c)\right]}{\sinh\left[\frac{(2n+1)\pi c}{b}\right]} \times \\ \times \sin\left[\frac{(2n+1)\pi}{2b}(y+b)\right] \quad (6)$$

Finally, the flow rate per unit cross-section is given by

$$\bar{u} = \frac{\varepsilon E_0 \langle \bar{\psi} \rangle}{4\pi\mu} \quad (7)$$

where $\langle \cdot \rangle$ indicates the average in the axial direction, *i.e.* $\langle \dots \rangle = L^{-1} \int_0^L (\dots) dx$, and a bar over a variable indicates its average over the cross-section. The induced pressure gradient can be computed from

$$\frac{dp}{dx} = \frac{\mu}{\bar{u}_p} \left[\frac{\varepsilon E_0 \bar{\psi}}{4\pi\mu} - \bar{u} \right] \quad (8)$$

The quantities $\bar{\psi}$ and \bar{u}_p in Eqs. (7) and (8) are given by the formulas:

$$\bar{\psi} = -\frac{\zeta_{AB}(x) + \zeta_{CD}(x)}{2} + \frac{b}{c} [\zeta_{AB}(x) + \\ + \zeta_{CD}(x) - \zeta_{BC}(x) \zeta_{DA}(x)] S_3(b, c) \quad (9)$$

and

$$\bar{u}_p = \frac{b^2}{3} - 2\frac{b^3}{c} S_5(b, c) \quad (10)$$

where the quantities S_3 and S_5 are defined as

$$S_3(b, c) = \left(\frac{2}{\pi}\right)^3 \sum_{n=0}^{\infty} \frac{1}{(2n+1)^3} \tanh[(2n+1)(\pi c/2b)] \quad (11)$$

$$S_5(b, c) = \left(\frac{2}{\pi}\right)^5 \sum_{n=0}^{\infty} \frac{1}{(2n+1)^5} \tanh[(2n+1)(\pi c/2b)] \quad (12)$$

4 Computational method

The incompressible steady-state Navier-Stokes equations were solved for the rectangular channel, using the Helmholtz-Smoluchowski slip boundary conditions for infinitely thin Debye layers. The equations were discretized using a finite volume method that employs a staggered grid for meshing the velocity components and pressure. The discretized equations were solved by the SIMPLER (Semi Implicit Method for Pressure Linked Equations Revised) algorithm discussed in [7]. The reader is referred to [8] for further details of the solution procedure.

The grid size was $\Delta z/2b = \Delta y/2b = \Delta x/4b = 0.05$ in Cases A to D, and, the boundary conditions at the entrance and exit planes of the duct involved the prescription of pressure following an approach substantially similar to that described in [11]. In Case E, as mentioned earlier, periodic boundary conditions were used on the velocity components and pressure. The grid resolution was $\Delta z/2b = \Delta y/2b = \Delta x/2b = 0.0067$ for the case $\lambda = (2b)/12$ and $\Delta z/2b = \Delta y/2b = \Delta x/2b = 0.02$ for the remaining cases.

5 Results of computation

Figure 2 shows the electroosmotic mobility μ_{eof} normalized by the reference mobility $\mu_{\text{eof}}^{\text{ref}}$ for Case A. These quantities are defined in Section 2 and may be calculated using the formulas presented in Section 3. The monotonic increase of $\mu_{\text{eof}}/\mu_{\text{eof}}^{\text{ref}}$ with ζ_1/ζ_0 is expected, since a higher zeta-potential corresponds to higher slip velocities. The sensitivity of the flow to changes in ζ_1/ζ_0 depends on the aspect ratio c/b , decreasing with increasing values of c/b . This is because when c/b is large, the face with the different ζ potential, $\zeta = \zeta_1$ is further removed from the bulk of the solution and consequently has a smaller effect on the overall fluid flux. The numerical results agree very well with the theory. This is to be expected, since when there are no axial variations at all, the asymptotic solution based on “slow” axial variations becomes exact.

The dimensionless form of the negative pressure gradient π_* , (defined by Eq. 3) is shown in Fig. 3 for Case B. The π_* calculated from the asymptotic theory using Eq. (8) is also in good overall agreement. Figure 4 shows the corresponding mobility data $\mu_{\text{eof}}/\mu_{\text{eof}}^{\text{ref}}$ both for Case B as well as Case C as a function of the dimensionless parameter αL . The asymptotic theory is expected to be reliable until about $\alpha \sim (2\pi)/(2b)$, that is, for $\alpha L \sim 2\pi(L/2b) \simeq 120$, and indeed this is consistent with Fig. 4.

Figures 5 and 6 show the normalized pressure gradient, π_* , for the long ($\lambda = L$) and short ($\lambda = L/10$) wavelength cases of Case D with $\Delta\zeta/\zeta_0 = 0.5$. The short wavelength

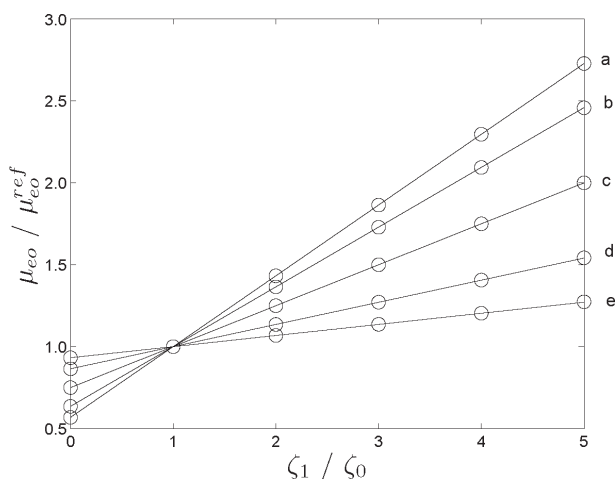


Figure 2. Electroosmotic mobility for Case A as a function of ζ_1/ζ_0 for various aspect ratios c/b . The curves labelled “a”, “b”, “c”, “d” and “e” are obtained for aspect ratio $c/b = 0.25, 0.5, 1, 2$ and 4 , respectively. The symbol “o” denotes the numerically calculated result and the solid line denotes the corresponding result from asymptotic theory.

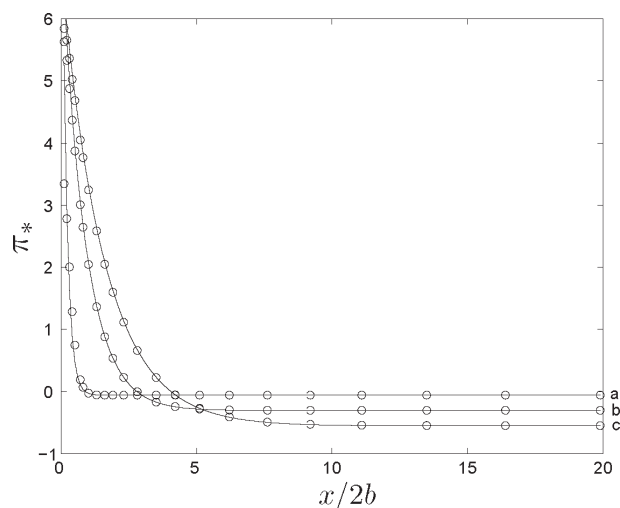


Figure 3. Dimensionless negative pressure gradient (π_*) as a function of $x/2b$ for Case B. The curves labelled “a”, “b” and “c” are obtained for $\alpha L = 115.13, 23.03$ and 12.79 , respectively. The symbol “o” denotes the numerically calculated result and the solid line denotes the corresponding result from asymptotic theory.

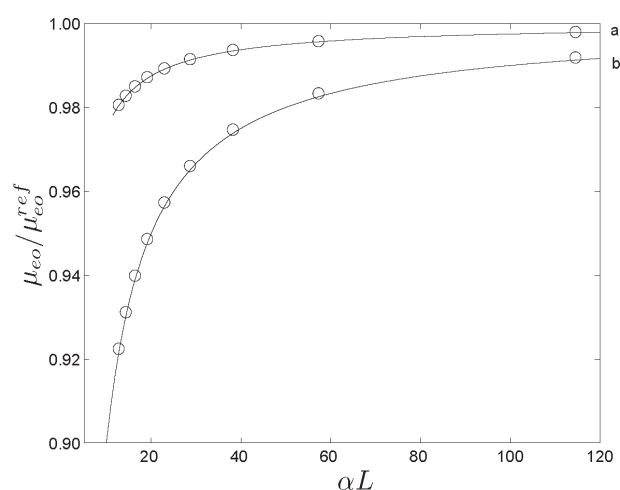


Figure 4. Electroosmotic mobility for Case B, indicated as curve (a) and for Case C indicated as curve (b) as a function of αL . The symbol “o” denotes the numerically calculated result and the solid line denotes the corresponding result from asymptotic theory.

case corresponds to $\lambda = L/10 = 4b$, so that the lubrication approximation is only marginally satisfied. In both cases however the induced pressure gradient is very accurately predicted. Figures 7 and 8 show the normalized velocity u/u_0 (Panel A) at four different axial locations indicated by the symbols in Figs. 5 and 6. In the long wavelength case, the agreement with the theory is excellent but in the short wavelength case, slight discrepancies – of the order of 1% – is seen.

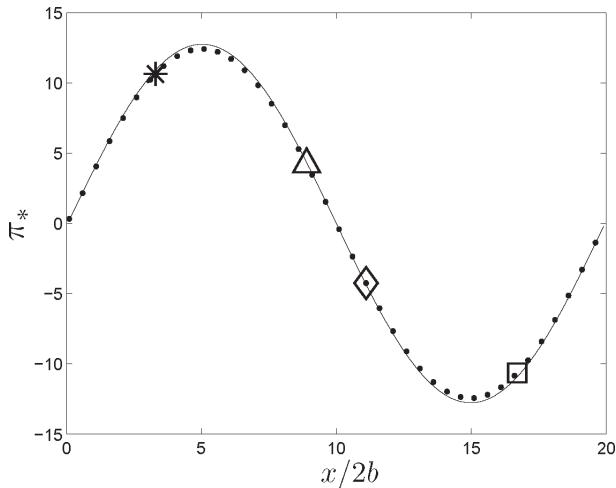


Figure 5. Dimensionless negative pressure gradient (π_*) as a function of $x/2b$ for Case D with $\lambda = L$ and $\Delta\zeta/\zeta_0 = 0.5$. The dots indicate numerically calculated results and the solid line corresponds to the calculation based on asymptotic theory. The points marked *, Δ , \diamond and \square denote the streamwise locations $x/2b = 3.3, 8.9, 11.1, 16.7$ for which velocity profiles are indicated by the corresponding symbols in Fig. 7.

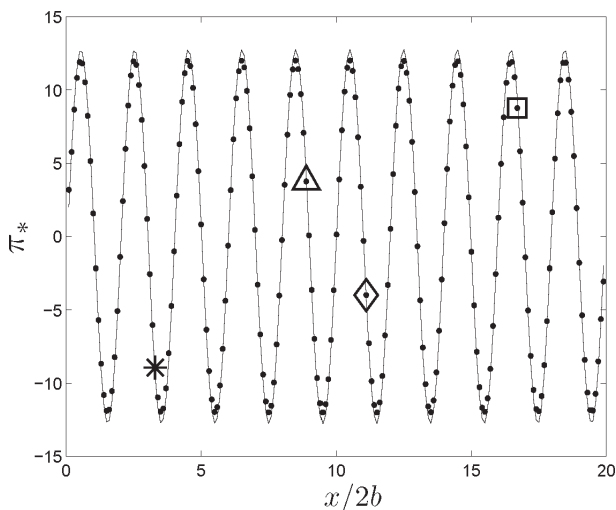


Figure 6. Same as Fig. 5 except that $\lambda = L/10$ and corresponding velocity profiles are in Fig. 8.

Equation (4) in Section 3 could be easily inverted (noting that if p does not depend on y and z then $p = \bar{p}$) and written in the form:

$$u_p = \mu \left(\frac{\varepsilon E_0 \psi}{4\pi\mu} - u \right) \left(\frac{d\bar{p}}{dx} \right)^{-1} \quad (13)$$

If Eq. (6) is used to evaluate ψ and the computed numerical results are used for u and \bar{p} in Eq. (13), then this quantity, which can be given the physical meaning of “pressure driven part of the flow per unit pressure gra-

dent” is a useful quantity to compare with theory. Indeed, in the lubrication limit, u_p is expected to be independent of everything but the channel geometry and should be given by Eq. (5). Panel B in Figs. 7 and 8 compares u_p extracted from the data [Case D with $\Delta\zeta/\zeta_0 = 0.5$] in this way with Eq. (5). In both cases there is collapse of the data onto the curve, though the agreement is much better in the long wavelength limit (Fig. 7) compared to the short wavelength case (Fig. 8). Since the smallness of $\lambda/(2b)$ is a measure of the accuracy of the lubrication approximation, this is consistent with expectations.

Figure 9 is the same as Panel B in Figs. 7 and 8 except that we vary the amplitude of the sine wave in Case D while keeping the wavelength fixed at $\lambda = L/5$. The amplitude $\Delta\zeta/\zeta_0$ is varied from 0.25 to 4. The quantity u_p defined in Eq. (13) is plotted as a function of $z/(2b)$ for $y = 0$ at two axial locations: $x/2b = 9.8, 10.3$. The theoretical curve, Eq. (5) is shown by the solid line. The collapse of the data onto the theoretical curve is very good, even though the amplitude $\Delta\zeta/\zeta_0$ is not small. This is to be expected, since the lubrication theory is based on long axial length scales, not small fluctuations in ζ . The deviation from the lowest order asymptotic theory however does depend on the amplitude, and generally the error increases with the amplitude of the fluctuations. This is indeed what is seen in Fig. 9.

It is easily verified from Eq. (7) that for Case D, the fluctuating part of the zeta-potential does not contribute to the volume flux of fluid. Thus, for Case D, we expect $\mu_{\text{eof}}/\mu_{\text{eof}}^{\text{ref}} = 1$. This was indeed observed in all cases run for Case D. Deviations from unity only appeared in the third or fourth decimal places and consequently could not be distinguished from numerical truncation errors.

In Figs. 10–12 the symbols indicate the computed velocity profiles for Case E at several axial locations for $\lambda/(2b) = 1, 1/3$ and $1/12$. In Panel A the computed solution is compared with the lubrication theory result, Eq. (5). It is seen that while for $\lambda/(2b) = 1$ there is reasonably good agreement, the accuracy of the lubrication solution rapidly deteriorates with decreasing values of $\lambda/(2b)$. In particular, when $\lambda/(2b) = 1/12$, the lubrication solution is not even qualitatively correct. For such short wavelength oscillations in the ζ potential, the velocity perturbation is confined to a narrow region next to the wall. Since in the short wavelength case one would expect that the presence of the side walls at $y = \pm b$ would be irrelevant, one might expect that $b \rightarrow \infty$ might be a more useful approximation than the lubrication limit in describing this situation. Fortunately, an exact analytical solution is known for Stokes flow between parallel plates in the infinitely thin EDL limit [10]. In Panel B of Figs. 10–12 the computed solution is compared with the solution repre-

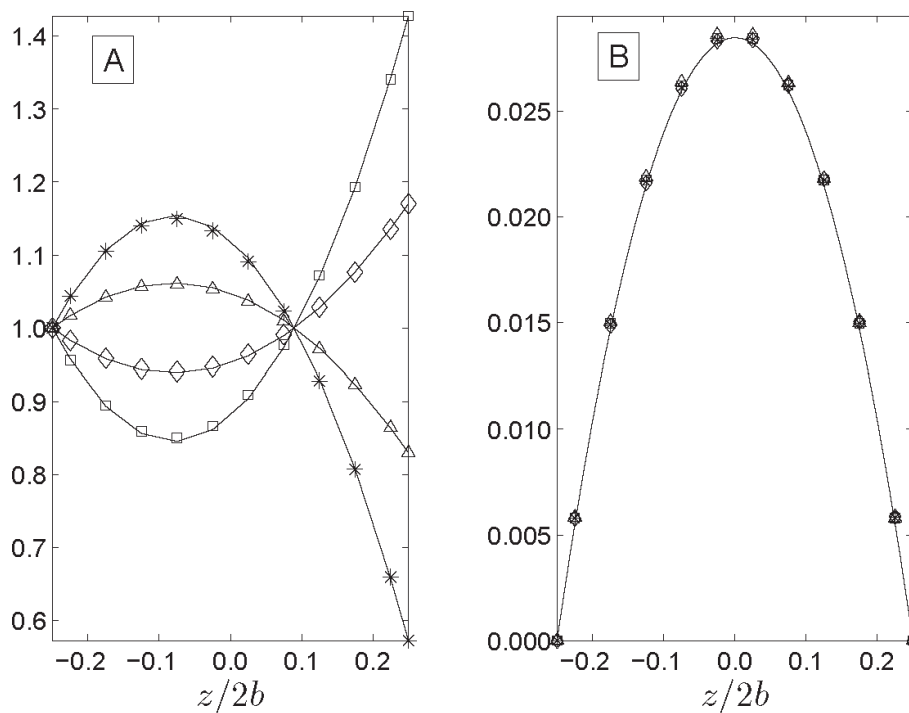


Figure 7. Panel (A) shows the streamwise velocity profiles $u(y = 0, z)/u_0$ for Case D with $\lambda = L$ and $\Delta\zeta/\zeta_0 = 0.5$ as a function of $z/(2b)$. Panel (B) shows the corresponding $u_p(y = 0, z)/(2b)^2$. The symbols: *, Δ , \diamond and \square , denote numerically calculated profiles at the streamwise locations indicated in Fig. 5. The solid line represents the corresponding profiles obtained from asymptotic theory.

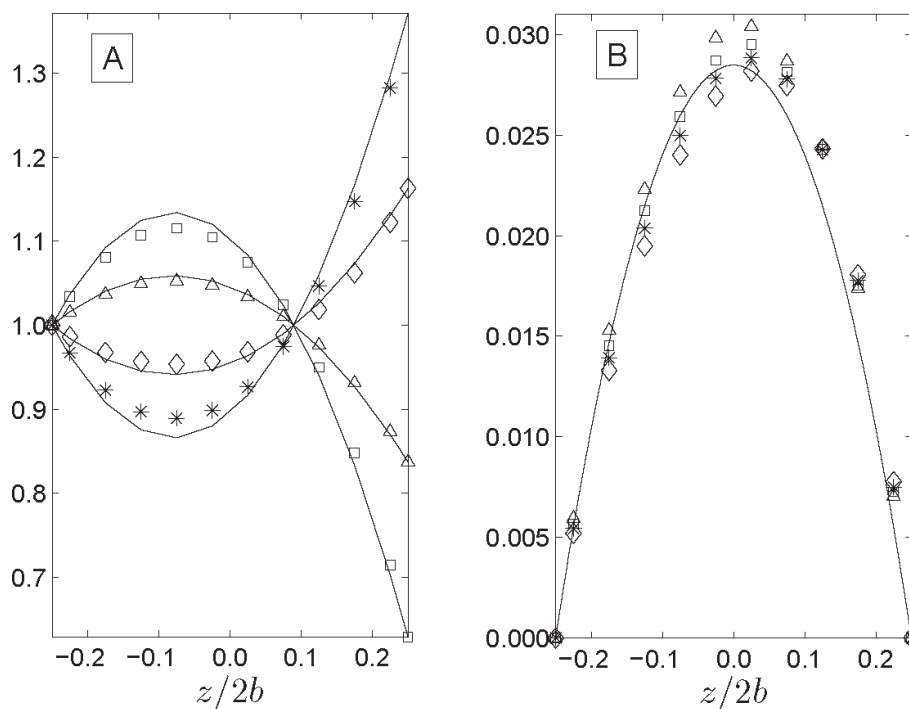


Figure 8. Same as Fig. 7 except that $\lambda = L/10$.

sented by Eqs. (9), (27) and (28) of [10]. These equations give the stream function for the velocity perturbation for a sinusoidal charge distribution in the cases where the sine waves on the upper and lower plates are (1) in phase and (2) out of phase. The present case of a single charged

plate can be generated by a linear superposition of these two solutions. It is seen that for $\lambda/(2b) = 1$, the computed solution agrees better with Ajdari's parallel plate solution than the lubrication theory of Section 3. Further, as $\lambda/(2b)$ is further reduced, the agreement with lubrication theory

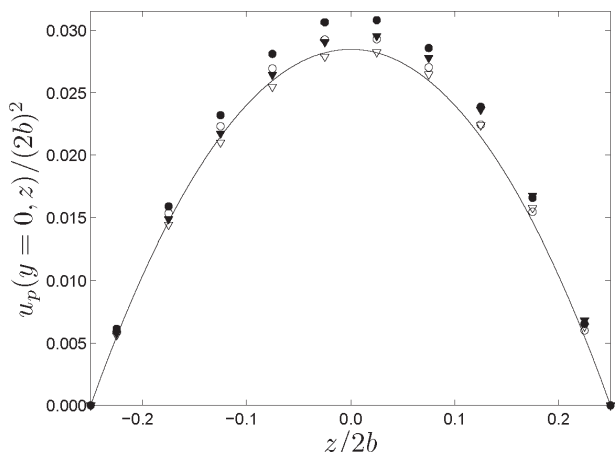


Figure 9. $u_p(0, z)/(2b)^2$ on the planes $x/2b = 9.8$ and $x/2b = 10.3$ for two different values of $\Delta\zeta/\zeta_0$ with $\lambda = L/5$ in Case D. The hollow and solid symbol of a given shape corresponds to $\Delta\zeta/\zeta_0 = 0.25$ and $\Delta\zeta/\zeta_0 = 4$, respectively. The round symbol corresponds to $u_p(0, z)$ on the plane $x/2b = 9.8$ and the triangular symbol corresponds to $u_p(0, z)$ on the plane $x/2b = 10.3$.

gets progressively worse while remaining in excellent accord with Ajdari’s solution. This is exactly the behavior one would expect, since the two theories are complementary in the sense that their respective zones of asymptotic convergence are $\lambda \gg (2b)$ (lubrication theory) and $\lambda \ll (2b)$ (Ajdari’s solution).

6 Conclusion

Numerical simulations of the incompressible Navier-Stokes equations were performed in a rectangular duct with spatially varying wall zeta-potential, constant electric field and zero pressure drop between channel inlet and outlet. The limit of infinitely thin EDL was assumed so that the effect of the wall zeta-potential could be handled in a simple manner through the artifice of the Helmholtz-Smoluchowski “slip boundary conditions”. Since Debye lengths are typically on the order of 10 nm compared to a channel width of 20 – 100 μm this is usually an excellent approximation in microfluidics. The effect of a spatial variation of the wall zeta potential on the electroosmotic flow was studied. Exponential and sinusoidal axial variations in the wall zeta potential was examined in the symmetric (all walls have the same zeta potential at a given axial location) as well as nonsymmetric cases.

Numerically calculated distributions of induced pressure gradients, flow rates and velocity profiles were compared with the corresponding analytical predictions based on lubrication theory with the objective of determining the limits of validity of the lubrication approximation. It was found that even though lubrication theory has formal validity only when the characteristic length scale for axial variations is much larger than the channel width, the predicted results were accurate to within a few percent even when the characteristic length scale was of the same order as the channel width. When fluctuations on a

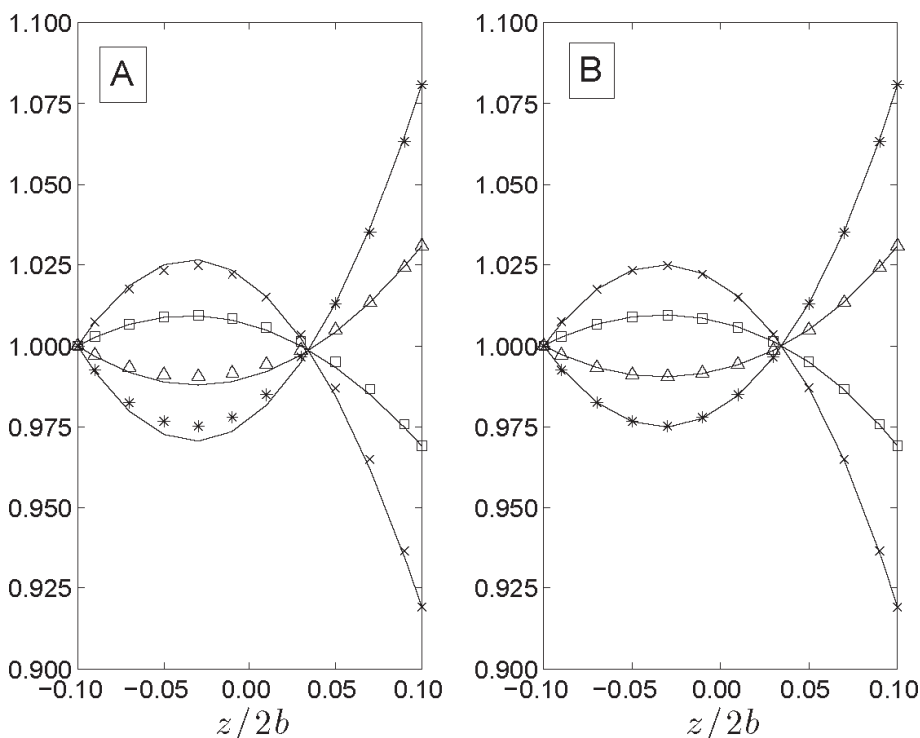


Figure 10. Panel (A) shows the streamwise velocity profiles $u(y = 0, z)$ for Case E with $\lambda/(2b) = 1$, $c/b = 0.2$ and $\Delta\zeta/\zeta_0 = 0.1$ as a function of $z/(2b)$ compared with the theoretical values calculated using Eq. (4). Panel (B) shows $u(y = 0, z)$ compared with the theoretical results presented by Ajdari [10]. The symbols: *, Δ , \diamond and \square denote numerically calculated profiles at the streamwise locations $x/2b = 0.1, 0.2, 0.6, 0.7$. The solid line represents the corresponding profiles obtained from the relevant theory.

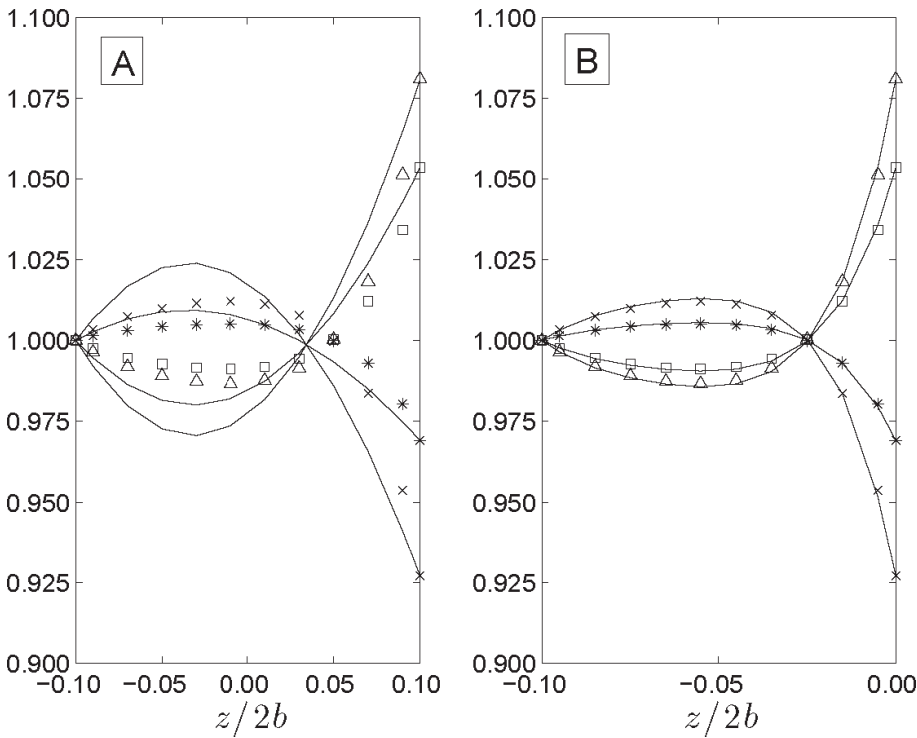


Figure 11. Same as Fig. 10 except that $\lambda/(2b) = 1/3$.

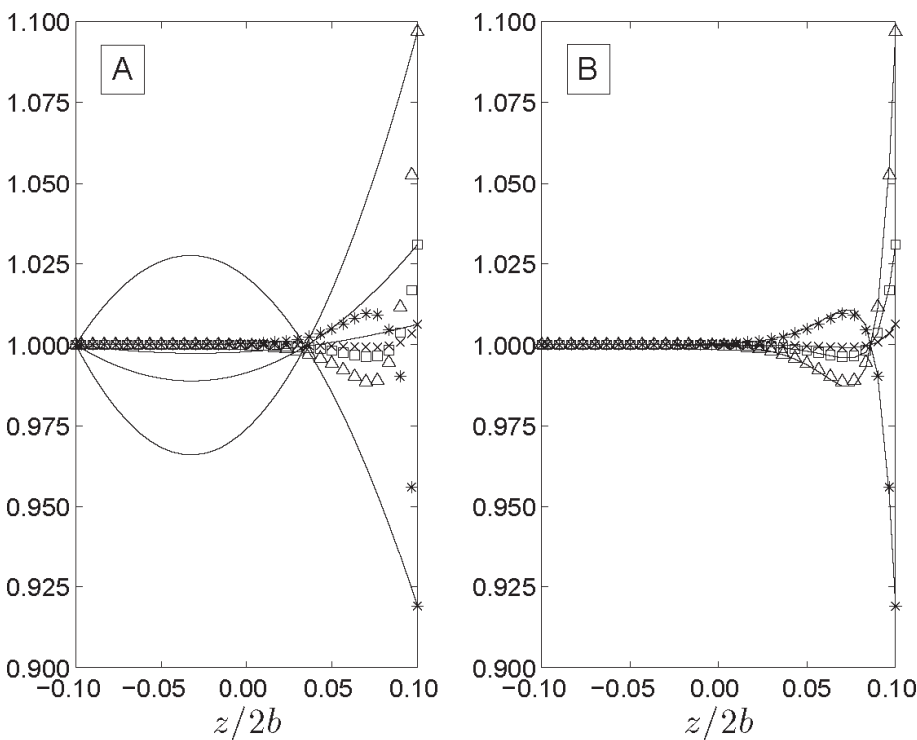


Figure 12. Same as Fig. 10 except that $\lambda/(2b) = 1/12$.

scale smaller than the channel width is considered, lubrication theory fails. This is also consistent with earlier studies of cylindrical capillaries [2]. The observed accuracy of lubrication theory, even when the formal condi-

tions for its validity are only marginally satisfied, is very encouraging because it suggests that lubrication theory could be used for obtaining analytical solutions for a wide variety of problems in microfluidics.

This “better than expected” performance however is neither surprising nor rare among asymptotic theories. In an asymptotic approximation, one only knows how the error scales with the expansion parameter but not the magnitude of the error itself [12]. Examples of asymptotic approximations exist on both sides of the spectrum: those that are accurate beyond all expectations as well as some that are so inaccurate as to be essentially useless for practical purposes.

SG was supported by the NSF under grant CTS-0330604.
NAP was supported by the NSF through the CAREER award (CTS-0134546)

7 References

- [1] Batchelor, G. B., *An Introduction to Fluid Dynamics*, Cambridge University Press, New York 1973, pp. 219–222.
- [2] Ghosal, S., *J. Fluid Mech.* 2002, 459, 103–128.
- [3] Ghosal, S., *Anal. Chem.* 2002, 74, 71–775.
- [4] Ghosal, S., *Electrophoresis* 2004, 25, 214–228.
- [5] Long, D., Stone, H. A., Ajdari, A., *J. Coll. Int. Sci.*, 1999, 212, 228–349.
- [6] Morrison, F. A. Jr, *J. Coll. Int. Sei.* 1970, 34, 45–54.
- [7] Patankar, S.V., *Numerical Heat Transfer and Fluid Flow*, Hemisphere Publishing Corporation, Washington 1980, p. 126.
- [8] Patankar, N. A., Hu, H. H., *Anal. Chem.* 1998, 70, 1870–1881.
- [9] Stone, H. A., Stroock, D. A., Ajdari, A., *Ann. Rev. Fluid Mech.* 2004, 36, 381–411.
- [10] Ajdari, A., *Phys. Rev. E*, 1996, 53, 4996–5005.
- [11] Versteeg, H. K., Malalasekera, W., *An Introduction to Computational Fluid Dynamics: The Finite Volume Method*, Prentice Hall, Harlow 1995, pp. 203–205.
- [12] Van Dyke, M., *Perturbation Methods in Fluid Mechanics*, The Parabolic Press, Stanford 1975, pp. 30–32.